Asociación Argentina
de Mecánica Computacional

Mecánica Computacional Vol XXX, págs. 3465-3478 (artículo completo)
Oscar Möller, Javier W. Signorelli, Mario A. Storti (Eds.)
Rosario, Argentina, 1-4 Noviembre 2011

CHARACTERIZATION OF AN ACTIVE MICROVALVE FOR GLAUCOMA USING FLUID-STRUCTURE INTERACTION

Fernando Sassetti[a,b], Fabio A. Guarnieri[a,b], Luciano Garelli[a,b] and Mario A. Storti[b]

[a]*Centro Internacional de Métodos Computacionales en Ingeniería (CIMEC), (INTEC-CONICET-UNL) Güemes 3450, (S3000GLN) Santa Fe, Argentina, http://www.cimec.org.ar*

[b]*Facultad de Bioingeniería, UNER, Ruta Prov. N^o 11 Km. 10, (3100) Oro Verde, Entre Ríos, Argentina, http://www.bioingenieria.edu.ar.*

Keywords: Glaucoma, Glaucoma Drainage Device, Finite Element Method.

Abstract. Glaucoma Drainage Device (GDD) have the potential to eliminate hypotony but still suffer from poor flow control and fibrosis. The ideal shunt should change its hydraulic resistance to achieve the desired intraocular pressure. In this work the characterization of a preliminary design of a new GDD is presented. This is activated by means of a diaphragm, which is actuated by conducting polymers. The valve can be manufactured employing Micro Electro Mechanical System (MEMS) technology by soft lithography. The characterization process is performed by numerical simulation using the Finite Element Method, considering the coupling between the fluid and the structure (diaphragm), obtaining the hydraulic resistance for several positions of the diaphragm. In order to analyze the hydraulic system of the microvalve implanted in a human eye an equivalent circuit model was used. The parameters of the equivalent circuit model were obtained from numerical simulation. The designed GDD has a greater range of variation of the hydraulic resistance if compared with the Ahmed valve. The proposed preliminary design allows to control intraocular pressure (IOP) by varying the hydraulic resistance in a greater range than existing passive valves and the numerical simulation facilitates the characterization and the improvement of the design before its construction, reducing time and costs.

1 INTRODUCTION

Glaucoma is the optic nerve damage often associated with increased of the IOP that leads to progressive and irreversible loss of vision. The aqueous humor (AH) is produced in the ciliary body behind the iris (in the posterior chamber), passes into the front of the eye (anterior chamber), and then exits through the drainage channels (See Fig.(1)). The AH leaves the anterior chamber primarily via the trabecular meshwork and it moves exteriorly into canal of Schlemm to the aqueous veins and then to the episcleral veins (Jacobs, 2009).

The IOP for general population is in the range 15.50±2.60 [mmHg] (Ethier and Ruberti, 2004). Ocular hypertension is defined when the IOP is higher than 20 [mmHg] in the absence of optic nerve damage or visual field loss, and is the most important risk factor for glaucoma. The treatment of glaucoma consists of topical or systemic IOP lowering agents or laser treatment. When these treatments are not effective, surgery is required and more complex cases require an implant of an aqueous shunt or GDD.

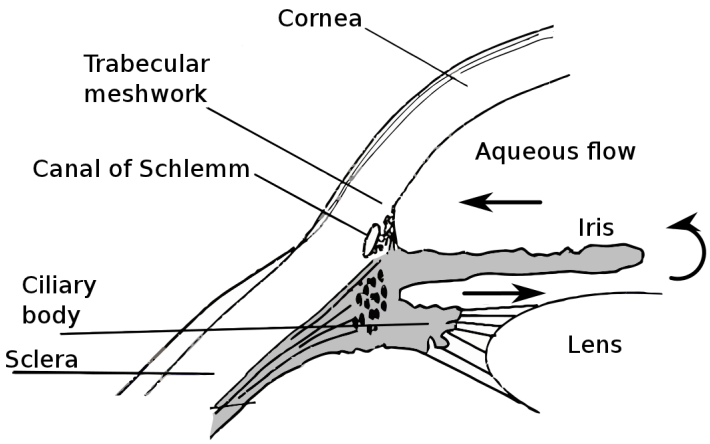

Figure 1: Aqueous humor formation and circulation. Figure adapted from (Humayun et al., 2007)

The shunts came into use in early 1900, when M. Rollet implanted a horse-hair connecting the anterior chamber to the sub-conjunctival space near the limbus. In 1969, Molteno introduced an external sub-conjuntival plate at the end of the tube shunt. This device and the others that are similarly used for AH drainage does not offer enough hydraulic resistance and they can originate complications related with the hypotony in the postoperative period. To reduce the effects of hypotony a flow resistor was added, such as the Ahmed Glaucoma Valve® (AGV). Another cause of failure of implants is associated with the increase of the IOP caused by the tissue-implant reaction (Hong, 2005). To avoid or diminish these problems, several modifications have been tried, like increasing plate area, substituting structural materials (Ishida et al., 2006), or inserting bypass resistances with micro tubes (Pan et al., 2005).

There have been attempts to replace the passive valves by active microvalves using electrochemical (Neagu, 1998; Pan et al., 2007) or electromagnetic actuators (Byunghoon, 2003), but several questions arise about biocompatibility and size issues.

Guarnieri describes in a patent (2007) an active implantable microvalve. The mechanism of the microvalve includes a diaphragm made of a conjugated polymer (CP) that shows high deformation and which volume depends from the electric potential applied to a pair of electrodes.

In recent years several methodologies have been proposed to simulate and characterize pas-

sive or active drainage devices (Neagu, 1998). In the work of Pan et al. (2003) two uncoupled models are used to characterize the AGV. First, the leaf displacement is obtained applying an evenly distributed pressure. Then, from the structural results, the geometry and the boundary conditions are established for the fluidic analysis. This is the simplest way to consider certain structural aspects on the fluid dynamics of the valve. A more complex model is presented by Stay et al. (2005), where the leaves of the AGV were modeled using the Von Karman plate theory, coupled to a Reynolds lubrication theory model of the AH flow through the valve, resulting in a two-dimensional coupled partial differential equation. In this model the governing equation are coupled in a monolithic way and presents some advantages over the modeling done by Pan et al. (2003), because the pressure distribution is given by the fluid dynamics of the problem. But one limitation is the inherent 2D geometry of the fluid domain to be simulated.

In this paper the characterization and simulation of the active microvalve proposed in Guarnieri (2007) for the treatment of glaucoma is presented. The perfomance of the microvalve is evaluated using tools from the computational mechanics and a circuit equivalent model.

2 MATERIALS AND METHODS

2.1 Active Microvalve

In Figure (2) a schematic diagram and the components that comprise the active valve are shown. The regulator was designed to control the IOP by varying its resistance to the AH flow, by means of the deflection of the diaphragm. The regulator is conceptually a normally closed valve, with a small leakage flow.

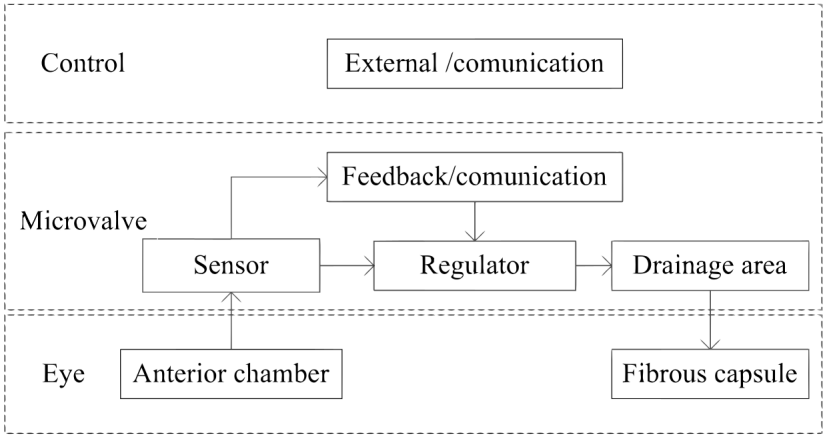

Figure 2: Schematic diagram of an active valve for glaucoma treatment.

The hydraulic resistance of the regulator has a passive component due to the effects of fluid pressure on the diaphragm and an active component due to the change in the geometry. When a voltage difference in the range of 1 [V] to 2 [V] is applied between the actuators' face, a deformation in the plane of the conjugated polymers in the range of 1% to 3% of its initials dimensions is produced (Smela, 1999). The deformation generates the bending of the diaphragm, decreasing the hydraulic resistance between the input and output channels.

In Figure (3) a cross section of the geometry of the regulator is shown. The channels (inlet and outlet) are connected by a deformable chamber. The valve structure is made of medical-grade silicone (Nusil, 2008). The use of these materials allows that the regulator can be manufactured using soft lithography.

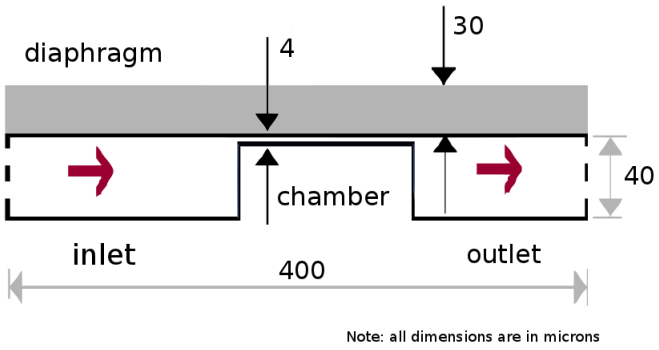

Figure 3: Geometry of the Regulator.

The actuator has a thickness of 30 [μm] and is composed mainly of a CP electrochemically deposited on a thin film conductor. The rigidity of the diaphragm is given by the properties of CP with a Young's modulus of 450 [MPa], which is greater than the 0.75 [MPa] of the silicone and the Poisson's ratios are 0.3 and 0.5 respectively.

2.2 Numerical model and simulation

In the presente work a fully coupled three-dimensional model is used. The AH is described by the incompressible Navier-Stokes equations, written in an arbritrary time dependent coordinate system. Eq.(1) express the conservation of mass for incompressible fluids and Eq.(2) the conservation of momentum.

$$\nabla \cdot \mathbf{v} = 0, \tag{1}$$

$$\rho \frac{\partial \mathbf{v}}{\partial t} + \rho[(\mathbf{v} - \mathbf{v}_m) \cdot \nabla]\mathbf{v} = \nabla \cdot \boldsymbol{\sigma} \tag{2}$$

where $\mathbf{v}$ is the fluid velocity, ρ the density, $\mathbf{v}_m$ the velocity of the moving reference frame and $\boldsymbol{\sigma}$ stress tensor (pressure and viscous forces). Assuming that the fluid is Newtonian its constitutive equation is given by

$$\boldsymbol{\sigma} = \tau - p\mathbf{I} \ \text{ with } \ \tau = \mu[\nabla\mathbf{v} + (\nabla\mathbf{v})^{\mathrm{T}}], \tag{3}$$

where μ the dynamic viscosity and p is the fluid pressure.In order to close the flow equations a set of boundary conditions are imposed

$$\begin{aligned} \boldsymbol{\sigma} \cdot \mathbf{n} &= \bar{\boldsymbol{t}} \ \text{ on } \ \Gamma_{\mathrm{N}}, \\ \mathbf{v} &= \bar{\boldsymbol{v}} \ \text{ on } \ \Gamma_{\mathrm{D}}, \end{aligned} \tag{4}$$

where Γ_N is a Neummann condition in the form of prescribed surface forces (tractions) and Γ_D is a Dirichlet condition where the velocity is imposed. For the structure a constitutive linear elastic solid assuming large displacements and rotations is adopted. The structure is described by the displacement vector $\mathbf{u}$, the velocity field $\mathbf{v}_s = \frac{\partial \mathbf{u}}{\partial t}$, the density of the material ρ_s and the Cauchy stress tensor $\boldsymbol{\sigma}_s$. Written in a Lagrangian description, with respect to the initial state Ω_s, we have

$$\rho_s \frac{\partial^2 \mathbf{u}}{\partial t^2} = \nabla \cdot \mathbf{P} \ \text{ in } \ \Omega_{\mathrm{s}}, \tag{5}$$

where the tensor $\mathbf{P} = J\boldsymbol{\sigma}_s\mathbf{F}^{-T}$ is called the first Piola-Kirchhoff tensor and $\mathbf{F} = (\mathbf{I} + \nabla\mathbf{u})$. For a convenient specification of the constitutive equation, the second Piola-Kirchhoff stress tensor

S is introduced and it is related to the first Piola-Kirchhoff stress tensor by $\mathbf{S} = \mathbf{F}^{-1}\mathbf{P}$. For an isotropic linear-elastic material, the constitutive equation can be stated as

$$\mathbf{S} = \lambda(tr\mathbf{E})\mathbf{I} + 2\mu\mathbf{E}, \tag{6}$$

which relates the second Piola-Kirchhoff stress tensor with the Green-Lagrange strain tensor **E** by means of the Lamé constants λ and μ. The Green-Lagrange strain tensor is defined as

$$\mathbf{E} = \frac{1}{2}\left(\nabla\mathbf{u} + \nabla\mathbf{u}^T + \nabla\mathbf{u}\cdot\nabla\mathbf{u}^T\right) \tag{7}$$

The coupling of this governing equations is carried out using a partitioned algorithm via fixed point iteration. For the fluid problem an Arbitrary Lagrangian-Eulerian (ALE) formulation is used in order to define a reference system following the moving boundaries while the structure is deformed.

The partitioned algorithm and the governing equations are implemented in the PETSc-FEM code (Storti et al., 2010), which is a parallel multiphysics finite element program based on MPI (the Message Passing Interface) and PETSc (the Portable Extensible Toolkit for Scientific Computations) library (Balay et al., 2011). The basic scheme considered in this work proceeds as follows:

1. Transfering the motion of the wet boundary of the solid to the fluid problem.
2. Updating the position of the fluid boundary and the bulk fluid mesh accordingly.
3. Advancing the fluid system and compute new pressures.
4. Converting the new fluid pressure (and stress field) into a structural load.
5. Advancing the structural system under the flow loads.

In this algorithm three codes CFD (Computational Fluid Dynamics), CSD (Computational Structure Dynamics) and CMD (Computational Mesh Dynamics) are running simultaneously. A schematic diagram is shown in Figure (4).

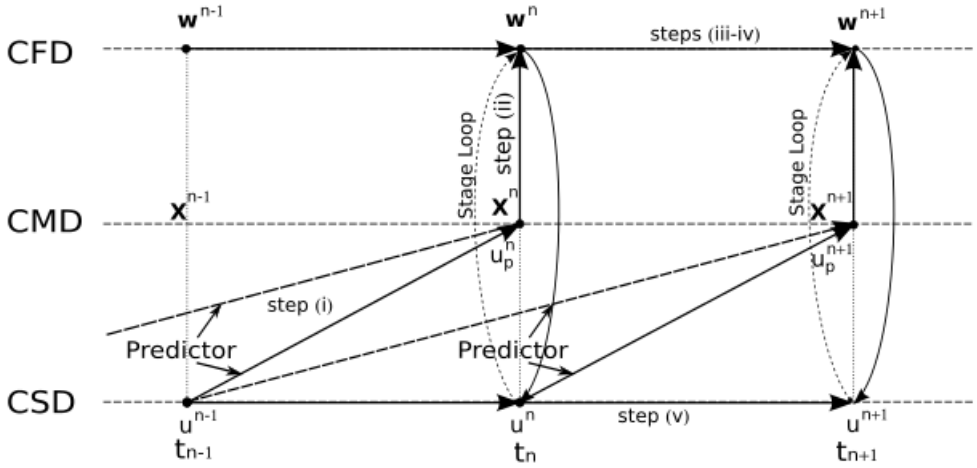

Figure 4: Synchronous FSI partitioned scheme

At time $\mathbf{t}_n$, we define $\mathbf{w}^n$ to be the fluid state vector $(\rho, \mathbf{v}, p)$, $\mathbf{u}^n$ to be the displacement vector (structure state vector) and $\mathbf{X}^n$ the fluid mesh node positions. For a more detailed description about the implementations of this coupling strategy can be viewed (Storti et al., 2009; Garelli et al., 2010).

This methodology allows to simulate both active and passive valves that have inherently three-dimensional flows. In the case of passive valves the fluid pressure deforms the diaphragm changing the hydraulic resistance and in the case of active valves the diaphragm deformation is prescribed as time function, changing the hydraulic resistance.

The PETSc-FEM code has been used previously in the resolution of problems in microfluidics and electrokinetic flows (Kler et al., 2009, 2010). Therefore, in order to validate the proposed coupling algorithm, the AGV is simulated with the geometry and mechanical properties described in Stay et al. (2005).

Only half of the AGV geometry was simulated due to its symmetrical nature, reducing the size of the discrete problem. The valve is discretized using a structured mesh with 37500 linear hexahedral elements for the fluid and 15000 linear hexahedral elements for the structure. The problem was solved for several pressure drops through the valve, in order to construct a flow rate curve.

Then, the characterization process of the active microvalve is carried out in two stages, first the passive resistance of the microvalve is obtained. In the second stage is analysed the active resistance of the microvalve, this is when the diaphragm is actuated. In this case the diaphragm is deformed and the hydraulic resistance is decreased due to a change in the geometry of chamber.

To carried out this simulation the microvalve was discretized using a structured mesh with 147920 linear hexahedral elements for the fluid and 137388 linear hexahedral elements for the structure. Only half of the structure mesh is shown in Figure (5) in order to obtain a clear view of the fluid mesh.

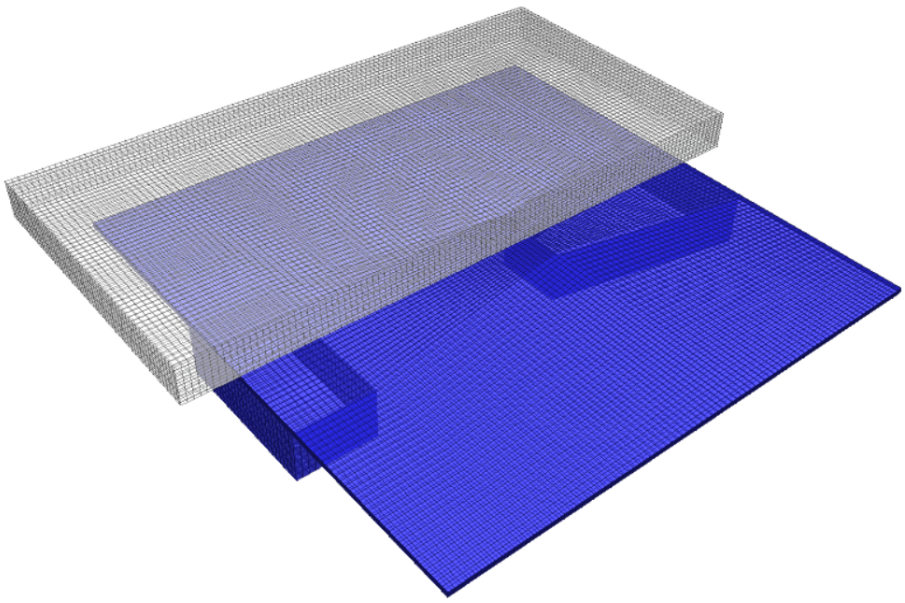

Figure 5: Structured mesh of the proposed microvalve.

To determine the variation in the passive hydraulic resistance of the microvalve due to fluid

pressure over the diaphragm, the flow rates were measured for different pressure drops. The outlet pressure was set at 8 [mmHg] and the entry ranged from 15 [mmHg] to 60 [mmHg]. For each case, the flow rate and the maximum displacement of the diaphragm were obtained. The active hydraulic resistance was calculated by setting a pressure drop of 7 [mmHg] in the microvalve, varying the position of the diaphragm due to a deformation of the conjugate polymer.

The numerical problem was carried out on a Beowulf cluster machine using 30 processors Intel®Pentium IV®Prescott 3GHz with 2 Gb of RAM, interconnected with two switch Gigabit Ethernet (1 Gbit/s), 3Com®Super Stack 3.

2.3 Equivalent Circuit Model

In order to analyze the hydraulic system of the microvalve implanted in a human eye an equivalent circuit model was used, which is shown in Figure (6) as proposed by (Pan et al., 2005). The circuit incorporates the effects of venous pressure and hydraulic resistance of the fibrous capsule that forms after the valve is implanted. The current source represents the generation of AH (2.5 [μL/min]) from the ciliary body of the eye; the capacitor depicts the capacity of the anterior chamber. Finally, the drainage is achieved on the episcleral vein at a pressure between 8 [mmHg] and 10 [mmHg] (Weinreb, 2007). The resistances of the model are represented by the hydraulic resistance of the microvalve (R_H) and the natural pathways of the eye (trabecular meshwork and uveoscleral outflow) (R_{OF}).

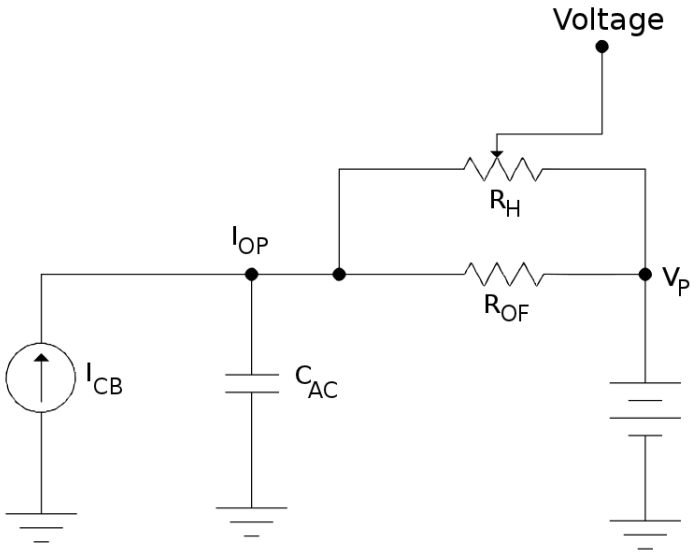

Figure 6: Equivalent circuit model.

In Table 1 is described the parameters used in the equivalent circuit.

The value of the I_{OP} was calculated at steady state.It is when the flow to entering the anterior chamber is equal to the output flow and the I_{OP} remains constant.

The AH passes through the hydraulic resistance to reach the drain, this resistance is calculated using Equation 8, where the R_H is obtained from the FEM simulation and the R_{OF} is in the range from 10 [mmHg·min/μl] to 100 [mmHg·min/μl] (Freddo and Johnson, 2008).

$$R_{EQ} = (R_H * R_{OF})/(R_H + R_{OF}) \tag{8}$$

Parameters	Description	Value
I_{OP}	Intraocular pressure	15 [mmHg]
I_{CB}	Flow ciliar body	2.5 [μl/min]
C_{AC}	Capacitor anterior chamber	—
V_P	Venous pressure	8 [mmHg]
R_{OF}	Outflow resistance	10-100 [mmHg·min/μl]
R_H	Microvalve Resistance	variable

Table 1: Equivalent circuit model parameters.

With the value of the equivalent hydraulic resistance the IOP was calculated using Equation 9, where V_P is the venous pressure and q is the flow of AH.

$$I_{OP} = V_P + R_{EQ} * q \tag{9}$$

3 RESULTS

In this section the results of the validation test and the characterization of the microvalve are shown. First, the passive hydraulic resistance is computed and then, the active hydraulic resistance. The equivalent circuit model is constructed using the obtained data from the previous simulations.

3.1 Validation Test

The results of the validation test proposed in Subsection § 2.2 are presented. The Table 2 shows the flow rate obtained by Stay et al. (2005) and Kara and Kutlar (2010) for AGV and they are compared with the results of PETSc-FEM.

The wall time to obtain a steady state solution was around 20 minutes using 30 processors Intel®Pentium IV®Prescott 3GHz. In the range of normal operation of the valve the flow rate is similar to that obtained by Stay et al. (2005) in their experiments.

Experimental		Stay et al.		Kara et al.		PetscFem	
Pressure [mmHg]	Flow rate [μl/min]	Pressure [mmHg]	Flow rate [μl/min]	Pressure [mmHg]	Flow rate [μl/min]	Pressure [mmHg]	Flow rate [μl/min]
5.20	1.54	5.80	1.55	5.37	1.6	5.80	1.90
7.40	2.51	6.52	2.51	7.74	2.5	7.01	3.81
8.51	4.95	7.71	4.96	8.51	5	8.00	5.87
9.70	9.97	9.21	9.98	9.25	10	9.00	8.71
10.50	19.95	11.02	19.96	11.29	20	11.00	17.80
10.81	24.91	11.64	24.98	11.82	25	11.50	20.00

Table 2: Hydraulic resistance of Ahmed Glaucoma Valve®.

3.2 Passive hydraulic resistance

In this subsection and the following, the results of the characterization process of the microvalve are presented. The Table 3 shows the flow rates for different pressure drops and can be concluded that the designed microvalve does not work as a passive pressure regulator, since the hydraulic resistance does not decrease with increasing IOP. The wall time to obtain the equilibrium state between pressure and elastic forces was around 25 minutes using 30 processors.

Intraocular Pressure [mmHg]	Displacement [μm]	Flow [μl/min]	Resistance [mmHg·min/μl]
15.00	0.024	0.54	13.08
22.50	0.049	1.12	12.96
30.00	0.074	1.72	12.80
37.50	0.100	2.32	12.72
45.00	0.125	2.94	12.59
52.50	0.151	3.56	12.50
60.00	0.176	4.20	12.38

Table 3: Passive hydraulic resistence.

In Figure (7) the pressure distribution is plotted jointly with the velocity field in the center plane of the microvalve for a pressure drop of 52[mmHg].

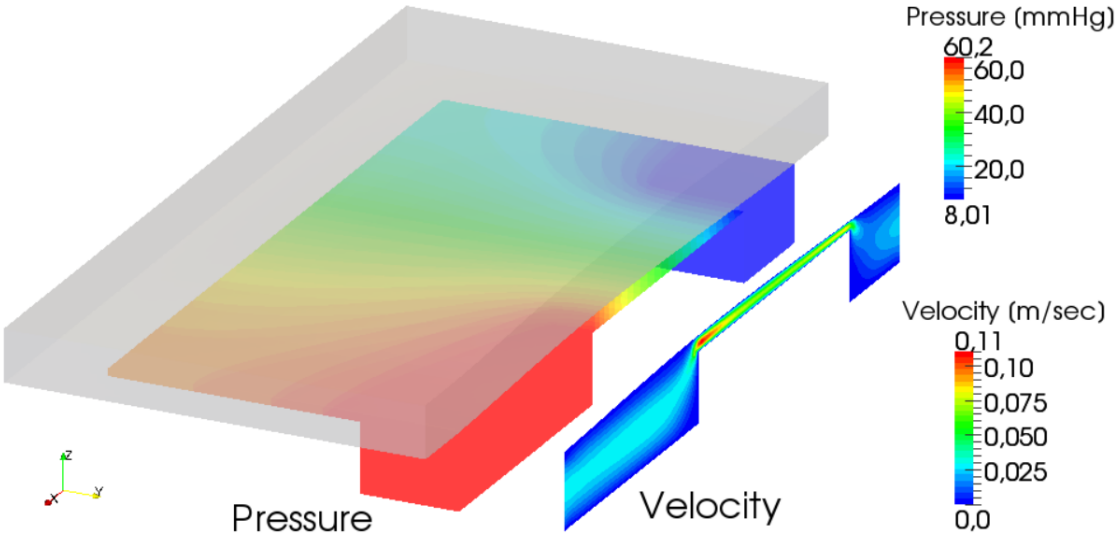

Figure 7: Pressure distribution and velocity field in the center plane.

3.3 Active hydraulic resistance

As was mentioned before, the application of a voltage to the actuator deforms the diaphragm. This deformation reduces the hydraulic resistance of the microvalve by increasing the area of passage between the input and output channels.

To characterize the change in the hydraulic resistance, the flow rate through the valve has been measured for a set of diaphragm deformations, fixing the pressure drop to 7 [mmHg]. The wall time to reach the steady steate was around 20 minutes using 30 processors.

In Table 4 the changes in the hydraulic resistance as a function of actuator deformation are shown. These results are used in §3.4 to obtain the IOP for different values of the hydraulic resistance of the regulator when episcleral pressure is 8 [mmHg] and the AH flow varies from 1 to 5 [μl/min].

The hydraulic resistance of the valve varies from 13.08 [mmHg·min/μl] to 0.36 [mmHg·min/μl] and the displacement of the diaphragm were in the range of 0 [μm] to 18.90 [μm]. In Figure

Deformation actuator [%]	Displacement [μm]	Aqueous flow [μl/min]	Resistance [mmHg·min/μl]
0.00	0.024	0.54	13.08
0.30	2.67	1.34	5.22
0.40	3.57	1.73	4.05
0.50	4.50	2.19	3.20
1.00	9.32	5.80	1.21
2.00	18.90	19.44	0.36

Table 4: Active hydraulic resistance.

(8) the streamlines for the maximum displacement of the diaphragm are shown and in Figure (9) is plotted the pressure distribution jointly with the velocity field in the center plane of the microvalve.

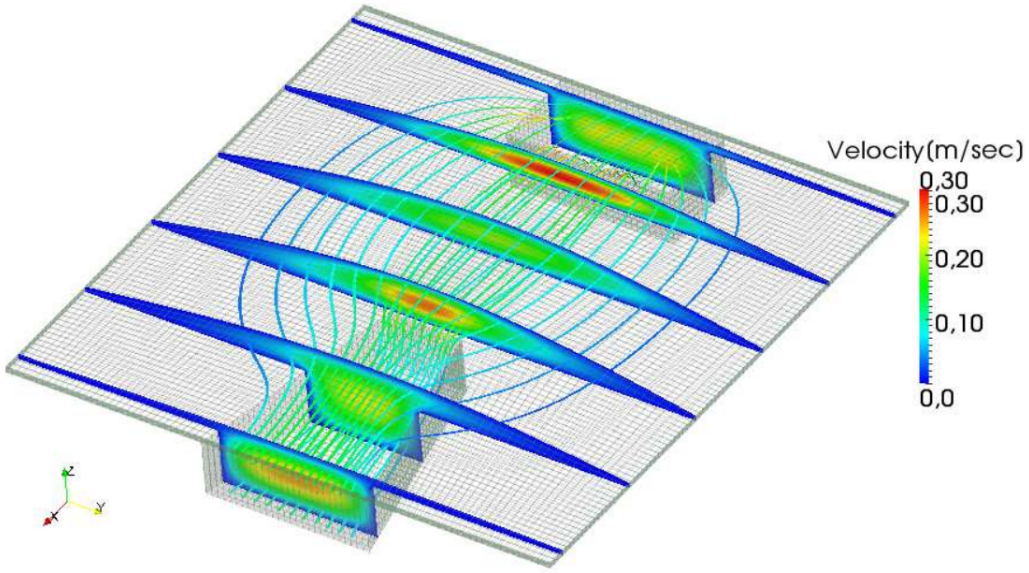

Figure 8: Streamlines for the maximum displacement of the diaphragm.

3.4 Equivalent circuit model

To analyze the hydraulic system of the microvalve an equivalent circuit model was used. In Table 5, possible values of the equivalent hydraulic resistance are presented. It was calculated for three cases of outflow resistance (R_{OF} = 10, 50, 100).The different combinations between R_{OF} and R_H can give an equivalent resistance in the physiological range of 3.2 [mmHg·min/μl] to 6.7[mmHg·min/μl] as noted by (Brubaker, 1997).

Figure (10) shows the values of IOP for different values of the hydraulic resistance of the regulator when episcleral pressure is 8 [mmHg] and the AH flow varies from 1 to 5 [μl/min]. The changes in the resistance of the regulator allow to control the IOP in a wide range, considering the flow rates in a physiological range.

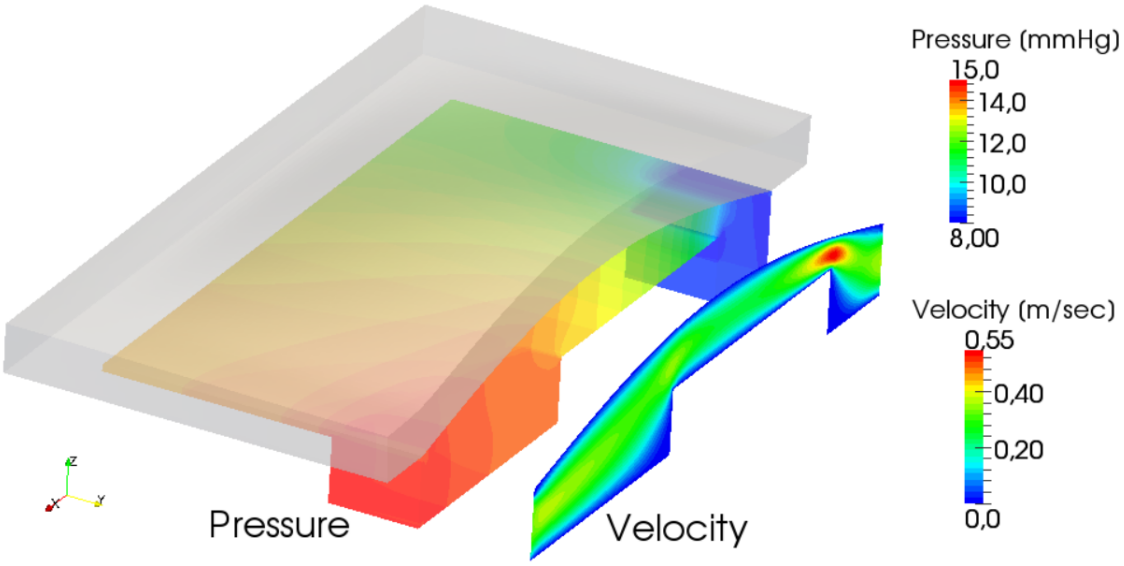

Figure 9: Pressure distribution and velocity field in the center plane.

R_H [mmHg·min/μl]		R_{OF} [mmHg·min/μl]	
	10	50	100
13.08	5.68	10.40	11.61
5.22	3.43	4.73	6.16
4.05	2.88	3.75	4.19
3.20	2.42	3.01	3.18
1.21	1.08	1.18	2.56
0.36	0.35	0.36	2.14

Table 5: Equivalent resistance.

4 DISCUSSION

The characterized and simulated microvalve, varies the hydraulic resistance by means of the deformation of a conductive polymer allowing the required control of IOP and reducing the fluctuations due to fluid structure interaction.The proposed regulation mechanism maintains a flow of AH similar to that of a healthy eye. The design has the advantage to change the hydraulic resistance and to adapt during the fibrous tissue encapsulation process, which often leads to increases in IOP as in the AGV®.

The microvalve has a passive hydraulic resistance of 13.08 [mmHg·min/μl] which is greater than the 3.38 [mmHg·min/μl] of the AGV®valve for flow rates around 2 [μl/min]. A passive resistance of 13.08 [mmHg·min/μl] prevents the risk of hypotony in the anterior chamber in the early stage of implantation, even when the flow of AH as low as 1 [μl/min], the IOP resulting is 18.40 [mmHg]. The dimensions of the actuator and the proposed regulator can withstand IOP around 60 [mmHg] without changing the passive resistance. The proposed design would improve the control of IOP in patient's eyes with different degree of glaucoma (10-100 [mmHg·min/μl]) and could regulate the IOP to the target in different situations in which the flow may vary from 1 [μl/min] to 5 [μl/min] during the day.

The use of FEM allows the modeling and analysis of fluid structure interaction of complex 3D geometries that would be difficult to resolve otherwise, enabling the improvement of the de-

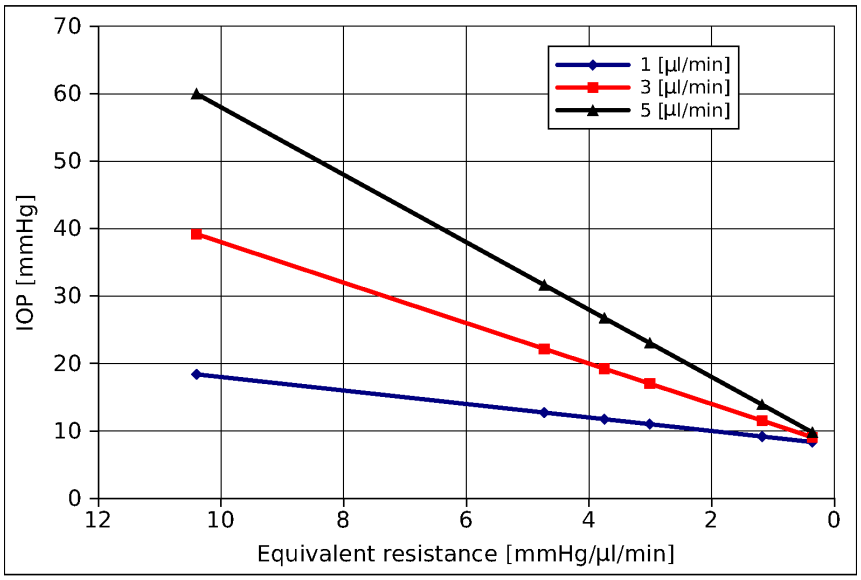

Figure 10: Intraocular pressure. $R_{OF} = 50$

sign before its construction, reducing time and costs. It also facilitates the calculation of active and passive resistance of the regulator to incorporate in the equivalent circuit model.The parallel computation allows to compute efficientely the problem reducing dramatically the calculus time (from day to minutes).

The coupling algorithm used in this work, in contrast with that used by Kara and Kutlar (2010) takes into account the mechanical properties of the elastomer and the geometric changes of the valve during the deformation process. The FSI scheme allows to solve the problem using both weak or strong coupling. In this work, the flow characteristics and the stiffness of the membrane makes it sufficient to use a weak coupling strategy, without instability problems. The equivalent circuit have allowed us to simulate the designed regulator and its interaction with the ocular hydraulic system.

ACKNOWLEDGEMENTS

This work has received financial support from Consejo Nacional de Investigaciones Científicas y Técnicas (CONICET, Argentina), Extensive use of freely distributed software such as GNU/Linux OS, MPICH, PETSc, Octave, ParaView and many others is done in this work.

REFERENCES

Balay S., Buschelman K., Gropp W.D., Kaushik D., Knepley M.G., McInnes L.C., Smith B.F., and Zhang H. PETSc Web pag. 2011.

Brubaker R.F. Clinical measurement of aqueous dynamics: Implications for addressing glaucoma. *Current Topics in Membranes*, 45:233–284, 1997.

Byunghoon B. In vitro experiment of the pressure regulating valve for a glaucoma implant. *Journal of Micromechanics and Microengineering*, 13:613–619, 2003.

Ethier C.R. Johnson M. and Ruberti J. Ocular biomechanics and biotransport. *Annual Review of Biomedical Engineering*, 6:249–273, 2004.

Freddo T.F. and Johnson M. Aqueous humor outflow resistance. *Current Topics in Membranes*, 62:161–192, 2008.

Garelli L., Paz R., and Storti M. Fluid-structure interaction study of the start-up of a rocket engine nozzle. *Computers & Fluids*, 39:7:1208–1218, 2010.

Guarnieri F.A. *Implantable ocular microapparatus to ameliorate glaucoma or an ocular overpressure causing disease*. 2007.

Hong C.H. Arosemena A.Z.D.A.R. Glaucoma drainage devices: a systematic literature review and current controversies. *Surv Ophthalmol*, 50(1):28–60, 2005.

Humayun M.S., Weiland J.D., Chader G., and Greenbaum E., editors. *Artificial Sight: Basic Research, Biomedical Engineering, and Clinical Advances*. Springer, 2007.

Ishida K., Netland P., Costa V., Shiroma L., Khan B., Ike I., and Ahmed K. Comparison of polypropylene and silicone ahmed glaucoma valves. *Ophthalmology*, 113:1320–1326, 2006.

Jacobs M.D. Multiscale systems integration in the eye. *Wiley Interdisciplinary Reviews: Systems Biology and Medicine.*, 1:15–27, 2009.

Kara E. and Kutlar A. Cfd analysis of the ahmed glaucoma valve and design of an alternative device. *Computer Methods in Biomechanics and Biomedical Engineering*, 13(6):655–662, 2010.

Kler P.A., Berli C., and Guarnieri F.A. Modeling and high performance simulation of electrophoretic techniques in microfluidic chips. *Microfluidics and Nanofluidics*, 10(1):187–198, 2010.

Kler P.A., López E.J., Dalcín L.D., Guarnieri F.A., and Storti M.A. High performance simulations of electrokinetic flow and transport in microfluidic chips. *Computer Methods in Applied Mechanics and Engineering*, 198(30-32):2360–2367, 2009.

Neagu C.R. *A medical microactuator based on an electrochemical principle*. Ph.D. thesis, Universiteit Twente, 1998.

Nusil. Med-6215 product profile. 2008.

Pan T., Baldi A., and Ziaie B. Remotely adjustable check-valves with an electrochemical release mechanism for implantable biomedical microsystems. *Biomedical Microdevices*, 9(3):385–394, 2007.

Pan T., Li Z., Brown J., and Ziaie B. Microfluidic characterization of a valved glaucoma drainage device with implications for enhanced therapeutic efficacy. In *Engineering in Medicine and Biology Society, 2003. Proceedings of the 25th Annual International Conference of the IEEE*, volume 4. 2003.

Pan T., Stay M., Barocas V., Brown J., and Ziai B. Modeling and characterization of a valved glaucoma drainage device with implications for enhanced therapeutic efficacy. *IEEE Transactions on Biomedical Engineering*, 52:948–951, 2005.

Smela E. Microfabrication of ppy microactuators and other conjugated polymer devices. *J.*

Micromech. Microeng., 9:1–18, 1999.

Stay M., Pan T., Brown J., Ziaie B., and Barocas V. Thin-film coupled fluid-solid analysis of flow through the ahmed glaucoma drainage device. *J. Biomech. Eng.*, 127(5):776–781, 2005.

Storti M., Nigro N., Paz R., Dalcin L., and Lopez E. Petsc-fem: A general purpose, parallel, multi-physics FEM program (1999-2010). http://www.cimec.org.ar/petscfem. 2010.

Storti M., Nigro N., Paz R., and Dalcín D. Strong coupling strategy for fluid structure interaction problems in supersonic regime via fixed point iteration. *Journal of Sound and Vibration*, 30:859–877, 2009.

Weinreb R.N. *Intraocular Pressure.* Kugler, 2007.